Petrographic and compositional indicators of formation and alteration conditions from LL chondrite sulfides

Devin L. Schrader[1*] and Thomas J. Zega[2]

[1]Center for Meteorite Studies, School of Earth and Space Exploration, Arizona State University, 781 East Terrace Road, Tempe, AZ 85287, USA.

[2]Lunar and Planetary Laboratory, 1629 E. University Blvd., University of Arizona, Tucson, AZ 85721, USA.

Geochimica et Cosmochimica Acta,
Volume 264, 1 November 2019, Pages 165–179

Reference:

Schrader D. L. and Zega T. J. (2019) Petrographic and compositional indicators of formation and alteration conditions from LL chondrite sulfides. *Geochim. Cosmochim. Acta* **264**, 165–179.

https://doi.org/10.1016/j.gca.2019.08.015

ABSTRACT

Sulfide minerals occur in many types of extraterrestrial samples and are sensitive indicators of the conditions under which they formed or were subsequently altered. Here we report that chemical and petrographic analyses of Fe,Ni sulfides can be used to determine the metamorphic type of the host LL chondrite, and constrain their alteration conditions. Our data show that the major- and minor-element compositions of the pyrrhotite-group sulfides (dominantly troilite) and pentlandite vary with degree of thermal metamorphism experienced by their host chondrite. We find that Fe,Ni sulfides in LL3 chondrites formed during chondrule cooling prior to accretion, whereas those in LL4 to LL6 chondrites formed during cooling after thermal metamorphism in the parent body, in agreement with previous work. High degrees of shock (i.e., ≥S5) caused distinct textural, structural, and compositional changes that can be used to identify highly shocked samples. Distinct pyrrhotite-pentlandite textures and minerals present in Appley Bridge (LL6) suggest that they cooled more slowly and therefore occurred at greater depth(s) in the host parent body than those of the other metamorphosed LL chondrites studied here. Sulfides in all LL chondrites studied formed under similar sulfur fugacities, and the metamorphosed LL chondrites formed under similar oxygen fugacities. The data reported here can be applied to the study of other LL chondrites and to sulfides in samples of asteroid Itokawa returned by the Hayabusa mission in order to learn more about the formation and alteration history of the LL chondrite parent body.

1. INTRODUCTION

Sulfides occur in many types of meteorites (e.g., Weisberg et al., 2006; Schrader et al., 2016) and are an important group of minerals because they are sensitive indicators of formation and alteration conditions in the Solar System. The compositions, textures, and crystal structures of sulfides can be used to constrain the oxygen and sulfur fugacites, and aqueous, thermal, shock, and cooling histories of their host rock (e.g., Arnold, 1967; Kissin and Scott, 1982; Schmitt et al., 1993; Bennett and McSween, 1996; Raghavan, 2004; Wang et al., 2006; Harries and Langenhorst, 2013; Schrader et al., 2016). The most abundant sulfides in extraterrestrial samples are the pyrrhotite group $(Fe,Ni,Co,Cr)_{1-x}S$ where $0 \leq x \leq 0.125$, which can occur with pentlandite $(Fe,Ni,Co,Cr)_9S_8$, Fe,Ni metal, and oxides such as chromite $FeCr_2O_4$ and magnetite Fe_3O_4 (e.g., Bullock et al., 2005; Tachibana and Huss, 2005; Jamsja and Ruzicka, 2010; Berger et al., 2011; Harries and Langenhorst, 2013; 2018; Harries and Zolensky, 2016; Schrader et al., 2016; 2018; Singerling and Brearley, 2018).

The crystal structure of the pyrrhotite-group sulfides can be described with a NiAs structure type, a hexagonally close-packed lattice in which Ni atoms occur in six-fold coordinated octahedral sites surrounded by As. The NiAs-type structure can adopt different polytypes due to stacking variations along the c-axis of the crystal. The stoichiometric end members are 2C (troilite; FeS, $x = 0$, hexagonal) and 4C (pyrrhotite; Fe_7S_8, $x = 0.125$, monoclinic). There are also modulated structures that are described in terms of ‘NC’, where ‘N’ designates the multiple of the superstructure in the c-axis dimension (e.g., Makovicky, 2006; Harries et al., 2011; Harries and Langenhorst, 2013). The NC-pyrrhotites with intermediate compositions (pseudo-hexagonal) include the integral 5C (Fe_9S_{10}, $x = 0.100$), 6C ($Fe_{11}S_{12}$, $x = 0.083$), and 11C ($Fe_{10}S_{11}$, $x = 0.091$) polytypes (e.g., Morimoto et al., 1975; Wang et al., 2006; Harries et al., 2011). Hence, the stoichiometry of the pyrrhotite-group sulfides are indicated by $Fe_{1-x}S$, where x varies between 0 and 0.125. Intergrowths of NC-pyrrhotites with 2C or 4C and 2C with 6C are common in terrestrial assemblages (e.g., Morimoto et al., 1975; Harries et al., 2011).

Pyrrhotite and pentlandite can form through high- and low-temperature processes (e.g., Raghavan, 2004). Pyrrhotite-pentlandite intergrowths can form via: (1) aqueous alteration (e.g., Brearley, 2006), (2) cooling of a primary high-temperature Ni-rich Fe-Ni-S melt with crystallization of monosulfide solid solution (mss) at ~950 °C (Fe,Ni-FeS eutectic; Kullerud, 1963b; McCoy et al., 2006) followed by pentlandite exsolution starting at ~610 °C, (3) thermal metamorphism of an Fe-Ni-S assemblage >610 °C and subsequent cooling, (4) annealing between ~600 and 200 °C (e.g., Kullerud, 1963a; Misra and Fleet, 1973; Francis et al., 1976; Etschmann et al., 2004), and (5) gas-solid sulfurization (Lauretta et al., 1998). After initial exsolution, the compositions of pyrrhotite and pentlandite can also change by low temperature (<100 °C) equilibration during slow cooling and/or annealing (Etschmann et al., 2004). While the upper temperature limit for pentlandite exsolution from mss is ~610 °C (e.g., Kullerud, 1963a), in the case of Fe-rich mss, exsolution of pentlandite can occur <610 °C (e.g., Naldrett et al., 1967; Misra and Fleet, 1973; Etschmann et al., 2004). The compositions of pyrrhotite and pentlandite that form through these myriad of pathways vary with equilibration temperature and thus can be used to constrain their origins (e.g., Kullerud, 1963a; Kullerud et al., 1969; Misra and Fleet, 1973; Francis et al., 1976; Naldrett, 1989; Karup-

Moeller and Makovicky, 1995; Sugaki and Kitakaze, 1998; Etschmann et al., 2004; Raghavan, 2004).

The pyrrhotite polytype, the presence of pentlandite, and the sulfide morphology further constrain the aqueous history, oxygen and sulfur fugacities, and shock history of the host rock. The pyrrhotite polytype in meteorites was found to vary with the degree of aqueous alteration, as the Fe/S ratio of pyrrhotite decreases with increasing degree of aqueous alteration; i.e., Fe/S of pyrrhotite in CM2 > CM1 > CI (Berger et al., 2011; Harries and Zolensky, 2016; Harries, 2018). The presence of pentlandite provides constraints on the minimum oxygen fugacity of the host rock (Schrader et al., 2016). The degree of shock a sample experienced on its parent body also affects the morphology of sulfides, which correlates with the shock stage of the silicates (Stöffler et al., 1991; Schmitt et al. 1993; Bennett and McSween, 1996).

Sulfides are present in both asteroids and meteorites, and so their comparison could yield valuable insights. Geothermometry of pyrrhotite-pentlandite intergrowths in highly unequilibrated (i.e., ≤3.2) meteorites shows that most formed via primary cooling from high temperature (i.e., during chondrule formation), while in equilibrated and thermally metamorphosed meteorites they formed via thermal metamorphism (e.g., Jamsja and Ruzicka, 2010; Schrader et al., 2015; 2016). Sulfides in LL3 chondrites are most likely primary, but may have experienced low-temperature secondary processing (Tachibana and Huss, 2005; Tachibana et al., 2006; Schrader et al., 2016; 2018). Sulfides in the LL4 to LL6 chondrites studied by Schrader et al. (2016) were argued to have equilibrated below 600 °C, consistent with formation after thermal metamorphism during cooling. Sulfides in an LL5/6 impact-melt breccia (Northwest Africa [NWA] 4859) analyzed by Jamsja and Ruzicka (2010) equilibrated ≤230 °C and the sulfides in the LL6 (S3) Stubenberg equilibrated <230 °C (Bischoff et al., 2017).

The timescales and location of sulfide thermal processing likely varied on the LL chondrite parent body. The equilibrated LL chondrites were heated on the order of 10 to 100 Ma (McCoy et al., 1991), and were thermally metamorphosed to temperatures up to ~950 °C (e.g., Slater-Reynolds and McSween, 2005; Nakamuta et al., 2017). Therefore, any primary, pre-accretionary, sulfides would have been significantly altered during thermal metamorphism. Sulfides may have also been altered via annealing at low temperatures during slow cooling over millions of years. The thermal histories (i.e., cooling rate) of LL chondrites do not trend with petrographic type, because their parent body was likely a rubble-pile (e.g., McSween and Patchen, 1989) rather than the well-stratified structure depicted in standard onion-shell models. In asteroids where the standard onion-shell model applies (e.g., Ganguly et al., 2013), deeply buried material was metamorphosed into type-6 material and cooled more slowly than the shallower and hence less heated type-5 and type-4 material, whereas unaltered type-3 material represents relatively ‘cold’ material at the asteroid’s surface. Since cooling histories do not trend with LL chondrites petrographic type, their sulfides may also record this complex thermal history.

Analyses of particles returned by the Japan Aerospace Exploration Agency mission Hayabusa, identified asteroid 25143 Itokawa as LL5 to LL6 chondrite material (~10% LL4 and ~90% LL5 to LL6; e.g., Nakamura et al., 2011; Tsuchiyama et al., 2011; 2014; Noguchi et al., 2014), which was thermally metamorphosed between ~780 and 840 °C (Nakamura et al., 2011). Itokawa particles were found to record shock stages between S2 and S4, with most particles around S2 (Noguchi et al., 2011; Zolensky et al., 2012). Sulfides are present in some Itokawa particles (e.g., Nakamura et al., 2011; Harries and Langenhorst, 2014; 2018; Berger and Keller, 2015), and may record additional information on the low-temperature formation conditions of asteroid Itokawa.

Here we report on petrographic and compositional indicators of sulfide formation conditions in LL3, LL4, LL5, and LL6 chondrites. Our goal is to constrain the conditions under which sulfides formed, and therefore the history of the LL chondrite parent body. The data reported here could be useful for interpreting the origins of sulfides in other LL chondrites, and in grains returned from asteroid Itokawa.

2. ANALYTICAL PROCEDURE

2.1. Mineralogy and petrology

Thin sections of LL3, LL4, LL5, and LL6 chondrite falls were initially characterized using an optical microscope to determine sample petrography, shock stage, and identify sulfides. An optical microscope was used to determine the shock stage of each sample using transmitted polarized light following the technique of Stöffler et al. (1991), and to verify the shock stage of samples reported in other studies. Backscatter electron (BSE) images and mineral identification via energy dispersive X-ray spectroscopy (EDS) were conducted on a JEOL JXA-8530F Hyperprobe electron probe microanalyzer (EPMA) at Arizona State University (ASU) and the Cameca SX-100 EPMA at the University of Arizona (UAz). We then selected pyrrhotite and pentlandite grains in Semarkona USNM1805-17 (LL3.00), Vicência ASU1996 (LL3.2), Hamlet ASU1194_C_2 (LL4), Soko-Banja USNM3078-1 (LL4), Chelyabinsk ASU1801_22_C1 (LL5), Siena USNM3070-3 (LL5), Appley Bridge USNM614-3 (LL6), and Saint-Séverin USNM2608-3 (LL6) for analysis (Table 1).

The major element compositions of sulfides, metals, olivine, and pyroxene were measured with the EPMA at UAz (Tables 2 and 3). Polished and carbon-coated thin sections were analyzed with a focused beam as individual points and line scans, with operating conditions of 15kV and 20 nA, and a ZAF correction method (a Phi-Rho-Z correction technique); peak and background counting times were varied per element to optimize detection limits. Some data for Semarkona (LL3.00), Soko-Banja (LL4), Siena (LL5), and Saint-Séverin (LL6) are from Schrader et al. (2016). Only stoichiometric sulfide and metal analyses with totals between 97.5–102.5 wt.%, and stoichiometric silicate analyses with totals between 98.0–102.0 wt.% were retained. Standards and detection limits are listed in Table 3 and Electronic-Annex [EA]-1.

2.2. Closure temperature, oxygen fugacity, and sulfur fugacity

2.2.1. Two-pyroxene temperature

Minimum metamorphic temperatures, estimated via two-pyroxene geothermometry, are known for Siena (LL5), Appley Bridge (LL6), and Saint-Séverin (LL6) (e.g., McSween and Patchen, 1989; Slater-Reynolds and McSween, 2005; Schrader et al., 2016). However, pyroxene equilibration temperatures for Appley Bridge (LL6) vary in the literature (e.g., McSween and Patchen, 1989; Slater-Reynolds and McSween, 2005), and so were recalculated here. The two-pyroxene equilibration temperature of Appley Bridge (LL6) was determined using the average compositions of low-calcium pyroxene (LCP) and high-calcium pyroxene (HCP) with the QUILF program (Anderson et al., 1993). Appley Bridge (LL6) is highly equilibrated, with LCP (this study; Table 3) and HCP (data from McSween and Patchen, 1989) being homogeneous, therefore average mineral compositions were used. The temperature was determined at a pressure of 1 bar; a reasonable approximation for an asteroid (e.g., Benedix et al., 2005). Pyroxene projections were computed using QUILF by considering both major and minor element compositions (e.g., Lindsley, 1983) for the average LCP and HCP compositions (Table 3). The two-pyroxene temperature for Appley Bridge was also calculated with the revised technique of Nakamuta et al. (2017), which added a kosmochlor component, and found to be within uncertainty of the value computed using QUILF.

2.2.2. Oxygen fugacity

The corresponding oxygen fugacity (fO_2) for Appley Bridge (LL6) was calculated at the appropriate two-pyroxene closure temperature of 913±36 ° C (2σ) (Table 3). The fO_2 was determined from the quartz-iron-ferrosilite buffer reaction (QIFs). The reaction equation is:

$$2Fe + 2SiO_2 + O_2 = 2FeSiO_3 \qquad (1).$$

The fO_2 for the reaction is determined via the following equation (for simplicity, ferrosilite, $FeSiO_3$, is expressed as Fs):

$$\log(fO_2)=2\log(a_{Fs}) - \log K - 2\log(a_{Fe}) - 2\log(a_{SiO2}) \qquad (2).$$

The online MELTS calculator (http://melts.ofm-research.org/CalcForms/index.html) was used to obtain the activity of ferrosilite (a_{Fs}) (Sack and Ghiorso, 1989; Hirschmann, 1991). The metal phase present at the two-pyroxene temperature was likely a homogeneous alloy (Harries and Langenhorst, 2018), therefore the bulk composition of Fe,Ni-metal was used to obtain the Fe activity (a_{Fe}) (Appley Bridge [LL6], a_{Fe} = 0.48; EA-1). The a_{Fe} value was determined from the molar Fe/(Fe+Ni+Co) content of bulk Fe,Ni metal, calculated using the modal abundances of Fe,Ni metal phases (98.2 vol.% taenite and 1.8 vol.% high-Co, low-Ni metal) as determined from thin section X-ray element maps in Adobe Photoshop ® using digital point counting (e.g., Schrader et al., 2014), and modal recombination analysis (e.g., Schrader et al., 2015). As discussed in Benedix et al. (2005) and Gardner-Vandy et al. (2013), based on experimental results of Larimer (1968) and modeling results of Matas et al. (2000) for the olivine-orthopyroxene-iron system, a silica activity (a_{SiO2}) of 0.9 is used in Eq. (2). The HSC 7.0 Chemistry Reaction Equation module was used to obtain the temperature dependent equilibrium constant (K) at 1 bar. Oxygen fugacities are referenced to the iron-wüstite (IW) buffer, which was also determined using HSC Chemistry. Alternative buffer systems could be used to calculate fO_2, however the same technique used here was used to determine the fO_2 for a wide range of meteorites (e.g., Benedix et al., 2005; Gardner-

Vandy et al., 2012; 2013; Schrader et al., 2013; 2017), including other LL chondrites (Schrader et al., 2016) that are discussed below, and for consistency and comparison with these studies we chose to use this same technique.

2.2.3. Sulfur fugacity

The sulfur fugacity (fS_2) for each meteorite was calculated from the chemical compositions of sulfide using an empirically derived 'Method 2' of Mengason et al. (2010), which is a revised version of the equation derived for fS_2 by Toulmin and Barton (1964). The revised method was used here because it accounts for Cu, which is present in sulfides studied here (Table 2). The equation to calculate fS_2 from the composition of sulfide is:

$$\log(fS_2) = (70.03 - 85.83N) \times (1000/T - 1) + 39.30 \times (1 - 0.9981N)^{1/2} - 11.91 \qquad (3).$$

Where T is the temperature in Kelvin, and N is the mol fraction of FeS (including Cu) in pyrrhotite from 'Method 2' of Mengason et al. (2010):

$$N = 2 \times ([nFe + nCu] / [nFe + 1.5nCu + nS]) \qquad (4).$$

Where n is in moles.

The fS_2 of each meteorite was calculated at the Fe-FeS eutectic temperature of 988°C (1261.15K) at one bar. The fS_2 value was then referenced to the iron-troilite (IT) buffer. Since there was only a trace abundance of pentlandite in all samples, except Appley Bridge (LL6), only the composition of Ni-poor pyrrhotite (Table 2) was used to determine fS_2 (as incorporating the composition of pentlandite would not alter the bulk composition). To calculate the fS_2 of Appley Bridge, because pentlandite is abundant within it, we used the bulk sulfide composition which was calculated using the modal abundances of sulfide phases (95.4 vol.% pyrrhotite and 4.6 vol.% pentlandite) determined from thin section X-ray element maps in Adobe Photoshop ® using digital point counting (e.g., Schrader et al., 2014), and modal recombination analysis (e.g., Schrader et al., 2015). The fS_2 values calculated are given in Table 4.

3. RESULTS

3.1. Shock stages

Shock stages of the samples in this study range from S1 to S5 (Table 1). The shock stage of S5 determined here for the thin section of Chelyabinsk (LL5) differs from that of its classification (S4; Ruzicka et al., 2015). However, shock stages of different pieces of the same meteorite can vary within ±1 (e.g., Bennett and McSween, 1996), and different lithologies of Chelyabinsk range from S3 to S4–5 material (Kaeter et al., 2018).

3.2. Sulfide textures and compositions, and associated opaque minerals

The morphologies of pyrrhotite-pentlandite intergrowths generally vary between meteorites (Figs. 1 and 2): lamellae of pentlandite occur within pyrrhotite in Semarkona (LL3.00) (Fig. 1a); blebs of pentlandite, sometimes with sharp grain boundaries, occur within pyrrhotite in Vicência (LL3.2) (Fig. 1b); blebs of pentlandite with islands of pyrrhotite occur in Hamlet (LL4) (Fig. 1c), Soko-Banja (LL4) (Fig. 1d), Chelyabinsk (LL5) (Fig. 1e), and Siena (LL5) (Fig. 1f); and blocky pentlandite in pyrrhotite occurs in Appley Bridge (LL6) (Fig. 1g) and Saint-Séverin (LL6) (Fig. 1h). Appley Bridge (LL6) also contains isolated regions of "mottled" pyrrhotite-pentlandite intergrowths bordering pentlandite, pyrrhotite, and/or Fe,Ni metal/metallic copper (Fig. 2b), a texture not seen in other LL chondrites studied here.

Based on major and minor element trends with Ni, Co, and Cu (Fig. 3), we define Ni-poor pyrrhotite as containing <1 wt.% Ni, Ni-rich pyrrhotite as containing between 1 and 16 wt.% Ni, and pentlandite as containing >16 wt.% Ni (Table 2; Schrader et al., 2016). Other solute elements occur in the sulfides and can be summarized as follows. Chromium occurs in pyrrhotite in LL3 and LL4 chondrites, while it is absent in LL5 and LL6 chondrites (Table 2). Copper occurs in pentlandite from all LL3, LL4, LL5, and LL6 chondrites, but it is highest in the LL5 Chelyabinsk (1.73±1.13 wt.% Cu, avg. ±std) and LL6 Appley Bridge (0.92±0.47 wt.% Cu) (Table 2). Cobalt occurs in pentlandite in all LL3, LL4, LL5, and LL6 chondrites studied, however it is typically below the EPMA detection limit (0.09 wt.% Co) in the LL5 Chelyabinsk (Table 2 and Fig. 3).

The ideal value for x in $Fe_{1-x}S$ (for Ni-poor pyrrhotite containing < 1 wt.% Ni) and polytypes are: 0 (FeS) = 2C; 0.125 (Fe_7S_8) = 4C; 0.100 (Fe_9S_{10}) = 5C; 0.083 ($Fe_{11}S_{12}$) = 6C; 0.091 ($Fe_{10}S_{11}$) = 11C; and NC is where $0<x<0.125$ but not near any of the integer values. The x values for Ni-poor pyrrhotite in all the samples reported here are approximately zero and so are compositionally consistent with troilite: Semarkona (LL3.00; $0.002<x<0.030$; n [number of analyses] = 33); Vicência (LL3.2; $0.001<x<0.028$; n = 23); Hamlet (LL4; $0.005<x<0.024$; n = 19); Soko-Banja (LL4; $0.005<x<0.030$; n = 38); Chelyabinsk (LL5; $0.003<x<0.027$; n = 22); Siena (LL5; $0.000<x<0.029$; n = 9); Appley Bridge (LL6; $0.000<x<0.011$; n = 12); and Saint-Séverin (LL6; $0.004<x<0.029$; n = 16). Therefore, we refer to Ni-poor pyrrhotite hereafter as troilite.

Ni-rich pyrrhotite (1<Ni<16 wt.%) in the samples (Table 2) has a range of Fe/S and cations/S ratios, where cations = Fe+Ni+Co+Cr+Al+Cu. These ratios span the range between the Fe/S ratios of troilite to the cations/S ratios of pentlandite (Fe/S = 0.828 to 0.980; cations/S = 0.984 to 1.158; Table EA-1). These compositions are not due to obvious beam overlap between troilite and pentlandite, as single mineral phases were targeted. However, we cannot be rule out that while analyzing troilite the interaction volume of the electron beam did not also sample pentlandite. It may be more likely that 'Ni-rich pyrrhotite' compositions are due to submicron pentlandite lamellae in the troilite that we could not resolve with the EPMA. If these analyses are not overlaps between troilite and pentlandite, these Ni-rich pyrrhotites could be polyphase assemblages of pyrrhotite. As their origin cannot be firmly established here, we do not rely on these analyses for geothermometry. Below we discuss sulfide morphologies and spatial relationships in each of the samples.

3.2.1. LL3 chondrites

Sulfides in Semarkona (LL3.00) and Vicência (LL3.2) are present in chondrules and the matrix. The sulfides are associated with kamacite and taenite and are dominantly troilite that contains minor pentlandite. In Semarkona, pentlandite textures occur as ‘flames’ and lamellae (Fig. 1a) within troilite. In Vicência, sulfides are associated with kamacite and taenite, and also contain pentlandite within troilite. Pentlandite in Vicência occurs as blebs within troilite, sometimes with sharp edges, which are typically along the edge of troilite grains (Fig. 1b).

3.2.2. LL4 chondrites

Sulfides in Hamlet and Soko-Banja are present in chondrules and the matrix, and are associated with kamacite and taenite, and are dominated by troilite that contains rare pentlandite. In Hamlet, pentlandite occurs as blebs and some contain islands of troilite, which are typically along the edge of troilite grains (Fig. 1c). In Soko-Banja pentlandite is present as blebs, which contain micron-sized islands of troilite, and occurs at the edge of larger troilite grains (Fig. 1d). One grain of MoS_2 was also found along the edge of a troilite grain (Schrader et al., 2016).

3.2.3. LL5 chondrites

Sulfides in Chelyabinsk and Siena occur in chondrules and the matrix, and are associated with kamacite and taenite, and are dominantly troilite with rare pentlandite. Troilite in Chelyabinsk appears to be polycrystalline in thin section under cross-polarized reflected light, with numerous grain boundaries visible in the thin section. Troilite grains contain numerous 120° triple junctions (Figs. 1e and 2a). Pentlandite in Chelyabinsk is present as blebs, typically near or along the edge of troilite grains. In rare cases, lens-like pentlandite is found along troilite grain boundaries. Pentlandite in Siena occurs as blebs, which contain islands of troilite (Fig. 1f).

3.2.4. LL6 chondrites

Sulfides in Appley Bridge are present in relict chondrules and the matrix, and are associated with tetrataenite, metallic Cu, and a high-Co, low-Ni metal (Figs. 1g and 2b, and EA-1); which is sometimes called cobaltian kamacite (e.g., cobalt-rich Fe,Ni metal; Chennaoui Aoudjehane et al., 2007) or wairauite [CoFe]. However, the metal is not pure CoFe as it contains Ni (63.8–71.2 wt.% Fe, 28.1–36.2 wt.% Co, and 0.55–1.5 wt.% Ni; EA-1), and the crystal structure of this high-Co, low-Ni metal is currently unknown (Rubin, 1990). The high-Co, low-Ni metal, and metallic Cu, are only seen at the interface between tetrataenite and sulfide (Figs. 1g and 2b), in a metal-sulfide assemblage that measures 6.4 x 7.4 mm. Large blocky pentlandite grains (up to 0.8 x 1.3 mm) along with troilite (4.1 x 7.1 mm) partially surround the grain of taenite (2.5 x 2.9 mm). The blocky pentlandite grains contain islands of troilite. There is a mottled morphology of pyrrhotite-pentlandite intergrowth at some boundaries between troilite and pentlandite grains (Fig. 2b).

Sulfides in Saint-Séverin occur in relict chondrules and the matrix, and are associated with kamacite and taenite. Rare pentlandite occurs as blebs and a blocky morphology, typically along the edge of sulfide grains, surrounded by troilite (Fig. 1h).

3.3. Oxidation and sulfidation states, and geothermometry

A two-pyroxene closure temperature, and corresponding fO_2, was determined for the equilibrated sample Appley Bridge (LL6) for comparison with data for Siena (LL5) and Saint-Séverin (LL6) from Schrader et al. (2016). Appley Bridge (LL6) has a two-pyroxene temperature of 913±36 °C (2σ), with a corresponding fO_2 of IW–1.7 (calculated using Eq. 2).

The fS_2 values for all meteorites studied here range from IT+0.8 to IT+2.3; at 988°C the log(fS_2) values range from -4.4 to -5.9 (Table 4; calculated using Eq. 3 and 4). There does not to appear to be any noticeable relationship between sulfide morphology, abundance of pentlandite, or petrographic type with fS_2. All meteorites have fS_2 values above the IT buffer, and are in the stability field of 6C pyrrhotite and troilite (see Figure 1a for T[°C] vs. log[fS_2] in Harries and Langenhorst, 2013).

The compositions of troilite and pentlandite within the LL chondrites studied here were compared to Fe-Ni-S phase diagrams available in the literature to determine their equilibration temperatures. We compare our data to Naldrett (1989) for reference to Fe-Ni-S phase stability between 100 to 135 °C; Misra and Fleet (1973) for reference to 230 °C and 300 °C; Craig et al. (1968) for reference to 400 °C; Shewman and Clark (1970) for reference to 500 °C; and Kosyakov et al. (2003) for reference to 600 °C (summarized in Raghavan, 2004). Sulfide compositions in the LL chondrites studied here are most consistent with equilibrating at or below 230 °C (Fig. 4), although equilibration down to 100 °C is possible. In the LL4 and LL5 chondrites, and the LL6 Saint-Séverin, pentlandite is generally richer in Ni than that in Semarkona (LL3.00) and Vicência (LL3.2) (Figs. 3 and 4, Table 2 and EA-1), perhaps indicating sulfide equilibration at higher temperatures. Sulfides in Appley Bridge (LL6) are consistent with equilibrating at or below 230 °C (Fig. 4g), potentially between 100 and 135 °C. To check these temperatures, the compositions of pentlandite in each of these meteorites were compared to phase relations in the Fe-Ni-S system developed via thermodynamic modeling (Waldner and Pelton, 2004; Waldner and Sitte, 2008), and consistent equilibration temperatures were found.

4. DISCUSSION

4.1. Indicators of the degree of thermal metamorphism, shock, and cooling history

The major and minor element compositions of pyrrhotite-group sulfides and pentlandite are generally correlated with the degree of thermal metamorphism experienced by the host meteorite (Fig. 3 and Table 2). However, the shock and cooling histories of the meteorites also affect the major and minor element compositions of both troilite and pentlandite. Therefore, chemical analyses of sulfides combined with petrographic observations can potentially be used to determine the metamorphic type and alteration conditions of the host LL chondrite. In each meteorite, Ni-poor pyrrhotite is compositionally consistent with being troilite (Table 2). Ni-rich pyrrhotite ranges in Ni content between troilite and pentlandite (Fig. 3), however without atomic-scale structural information the specific polytype(s) are unknown. These sulfides may be polyphase assemblages, and the sulfides with Fe/S ratios between 0.92 (6C pyrrhotite) and 1 (troilite) could be mixtures of 6C pyrrhotite and troilite (Table EA-1).

The Ni content of pentlandite in the LL chondrites may be an indicator of a trend in equilibration temperature (Table 2). The minimum Ni content of pentlandite generally trends with petrographic type, as it is lowest in both LL3 chondrites and the LL4 Soko-Banja (down to ~16 wt.% Ni; Table 2). However, there is no noticeable trend in the average Ni content of pentlandite with petrographic type (Table 2). This is consistent with the LL chondrite parent body being a rubble pile (e.g., McSween and Patchen, 1989). The lack of a trend between the average Ni content of pentlandite with petrographic type is also consistent with pentlandite in the LL5/6 impact melt NWA 4859 (avg. 16.4 to 17.1 wt.% Ni, between the two pentlandite morphologies; Jamsja and Ruzicka, 2010), and that in the LL6 Stubenberg (avg. 16.3 wt.% Ni). In experimentally formed pentlandite, which shows a range of Ni contents, the minimum Ni content of pentlandite decreases as the equilibration temperature decreases (Raghavan, 2004). The minimum Ni content of pentlandite is lowest in the LL3 chondrites and the LL4 Soko-Banja, and so our data suggest that these pentlandites equilibrated at a lower temperature than those in the higher petrographic type LL chondrites studied here. However, the closest match closure temperature for these three samples are all ≤230 °C (Figs. 4a,b,d).

The abundances of the minor elements Co, Cr, and Cu in troilite and/or pentlandite trend with petrographic type (Table 2 and Fig. 3). Chromium is present in troilite in LL3 and LL4 chondrites, whereas it is absent in LL5 and LL6 chondrites (Table 2). This is consistent with troilite in the LL3.1 Bishunpur that has up to 0.44 wt.% Cr (Lauretta et al., 2001; Tachibana and Huss, 2005), and the LL5/6 impact melt NWA 4859 with ~0.02 wt.% Cr (Jamsja and Ruzicka, 2010), which is the below the Cr detection limit of this study (0.02 – 0.03 wt.% Cr; EA-1). Similarly, troilite in the LL6 Stubenberg was found to have <0.02 wt.% Cr (Bischoff et al., 2017). While Cu is present in pentlandite from all LL3, LL4, LL5, and LL6 chondrites, it is highest in the LL5 Chelyabinsk (1.73±1.13 wt.% Cu; average±standard deviation) and LL6 Appley Bridge (0.92±0.47 wt.% Cu) (Table 2 and Fig. 3). Both samples are outliers; Chelyabinsk (LL5) has the highest shock stage (S5; Table 1) and Appley Bridge (LL6) sulfides have distinct pyrrhotite-pentlandite morphologies (Figs. 1g and 2b). Copper was not analyzed in pentlandite in either NWA 4859 (Jamsja and Ruzicka, 2010) or Stubenberg (Bischoff et al., 2017) for comparison here. Cobalt is also present in pentlandite in all LL chondrites studied here, however it is typically below the EPMA detection limit (<0.09 wt.% Co) in the LL5 Chelyabinsk (Table 2 and Fig. 3), perhaps a result of the high degree of shock this sample experienced; although the exact mechanism for this depletion is unknown. In contrast, pentlandite in the LL5/6 annealed impact melt NWA 4859 contains between 0.77 and 1.27 wt.% Co (Jamsja and Ruzicka, 2010). Therefore, if a depletion of Co in pentlandite can result from a high-pressure shock event (i.e., ≥S5), the lack of Co in pentlandite from Chelyabinsk but abundance in pentlandite from NWA 4859 might be because Chelyabinsk was not annealed.

4.1.1. Indicators of high shock stage

Chelyabinsk (LL5) displays petrographic evidence in its silicates and sulfides for having undergone a high-pressure shock event(s). By optical microscopy of its silicates, the thin section of Chelyabinsk (LL5) studied here is an S5, indicating a shock pressure of between 35 and 45 GPa (Stöffler et al., 1991). Troilite in Chelyabinsk (LL5) shows abundant 120° triple junctions (Figs. 1e and 2a), which were also noted by Kaeter et al. (2018) in different samples of Chelyabinsk (LL5). Troilite in samples of Kernouvé (H6) that were experimentally shocked at 35 GPa and 60 GPa is entirely polycrystalline with 120° triple junctions (Schmitt et al., 1993). Bennett and McSween (1996) observed that polycrystalline troilite with 120° triple junctions are primarily present in S5 and S6 L chondrites, although rare instances were found in S3 and S4 L chondrites. The peak temperature increase during an S5 shock event is between 350 and 600 °C. This temperature increase (even if from a pre-impact host rock temperature of 0 °C) is high enough to alter the pre-impact sulfide assemblage as the breakdown temperature of pyrrhotite-pentlandite intergrowths is ~610 °C and diffusion can continue during cooling to room temperature (e.g., Etschmann et al., 2004).

4.1.2. Distinct cooling history of Appley Bridge

Appley Bridge (LL6) contains a pyrrhotite-pentlandite intergrowth texture (i.e., mottled) and minerals that were not observed in the other seven LL chondrites studied here. It is possible that such textures and minerals are related to its low-temperature (≤230 °C) thermal history (Fig. 4g). Similar to that reported here in Appley Bridge (LL6), a high-Co, low-Ni metal associated with taenite, kamacite, and Cu was observed in Benguerir (LL6, S2) and Usti Nad Orlici (L6, S2) (Chennaoui Aoudjehane et al., 2007). Chennaoui Aoudjehane et al. (2007) argued the formation of the high-Co, low-Ni metal is due to low temperature (<200 °C) breakdown of a metastable Fe-, Cu-, and Co-bearing sulfide, and not the result of shock. Rubin (1990) also found the same high-Co, low-Ni metal in Appley Bridge (LL6) reported here, and argued that it formed during cooling below 325°C. However, Rubin (1990) noted that the high-Co, low-Ni metal in Appley Bridge (LL6) does not have enough Co (i.e., 28.1–36.2 wt.% Co; EA-1) to be considered wairauite (CoFe; ~49 wt.% Co), and needs structural analysis to determine if it is a new mineral or a solid solution between kamacite (Fe,Ni), which has a body centered cubic structure with a cell dimension (a_0) of a_0=0.286 nm (Frazer, 1969), and wairauite, which has a primitive cubic structure with a_0=0.2857 nm (Bayliss, 1990). The low-temperature formation of the high-Co, low-Ni metal in Appley Bridge (LL6) (perhaps <200 °C) is consistent with the equilibration temperature of sulfides in Appley Bridge (≤230 °C: Fig. 4g), and also indicates that the mottled pyrrhotite-pentlandite texture formed at low temperature.

Sulfides in all LL chondrites studied here equilibrated ≤230 °C, and so the distinct minerals and sulfide textures observed in Appley Bridge are likely not the result of low-temperature equilibration alone. We hypothesize that Appley Bridge had a distinct thermal history, perhaps cooling more slowly, than the other metamorphosed LL chondrites studied here. If Appley Bridge did cool more slowly than other LL chondrites studied here, it may have had the time needed for the distinct minerals to exsolve and sulfide textures to develop. If so, Appley Bridge may have been more deeply buried and therefore more thermally insulated on in its parent body during slow cooling (e.g., McCoy et al., 1991) than the other LL chondrites studied here.

4.2. Implications of geothermometry, and oxidation and sulfidation state

The two-pyroxene and sulfide geothermometries of the samples, combined with their parent body metamorphic temperatures, constrain the meteorites' thermal histories. The two-pyroxene temperatures are 867±28 °C (±2SE; standard error of the mean) for Siena (LL5), 899±70 °C (±2SE) for Saint-Séverin (LL6) (Schrader et al, 2016), and 913±36 °C (2σ) for Appley Bridge (LL6) (Table 3). Within uncertainties, all three temperatures are the same, and are similar to two-pyroxene temperatures of other LL5 and LL6 chondrites (e.g., Slater-Reynolds and McSween, 2005). The two-pyroxene temperature of Appley Bridge (LL6) determined here is almost identical to that of the LL6 Stubenberg (914±44 °C) determined by Bischoff et al. (2017), which was also determined using QUILF. These temperatures are the equilibration, or closure, temperatures of LCP and HCP, and represent minimum metamorphic temperatures of the LL chondrites. The peak metamorphic temperatures (PMT) of Semarkona (LL3.00) and Krymka (LL3.2) are <220 °C and <270 °C, respectively (Busemann et al., 2007). Assuming the PMTs of LL3.2 chondrites are similar, we infer that Vicência (LL3.2) was not heated above 270°C. However, the PMTs of Busemann et al. (2007) were determined from insoluble organic matter separates; the thermal histories of which may or may not be decoupled from the host rock, though it seems unlikely they were decoupled. In comparison, LL4 chondrites were thermally metamorphosed to temperatures >600 °C (McCoy et al., 1991). The sulfide-equilibration temperature for both Semarkona (LL3.00) and Vicência (LL3.2) of ≤230 °C (Fig. 4a,b) is similar to or higher than the parent-body metamorphic temperatures, assuming the thermal histories of insoluble organic matter and the host rock were coupled, which is consistent with sulfide formation after chondrule formation during cooling (e.g., Schrader et al., 2016; 2018). However, some sulfide grains in the LL3s indicate equilibration at lower temperatures (down to 100 °C), and therefore we cannot rule out that some sulfides in these samples were equilibrated at low temperatures, either during chondrule cooling or annealing on the parent body. In contrast, the sulfide equilibration temperatures of all LL4, LL5, and LL6 chondrites studied here (Figs. 4c-h) are below the minimum metamorphic temperatures they experienced on their parent body, indicating all of their sulfides were altered on the LL chondrite parent body and formed after thermal metamorphism during cooling (e.g., Schrader et al., 2016).

4.2.1. Oxidation and sulfidation state

The oxygen fugacity of formation influences the major and minor element composition of sulfides, and a minimum fO_2 of approximately IW–2.2 may be required for the formation of pentlandite (Schrader et al., 2016). Of all the LL chondrites studied here, Appley Bridge (LL6) formed under the most oxidizing conditions (IW–1.7) and contains the highest abundance of pentlandite. In comparison, Siena (LL5; IW–2.2) and Saint-Séverin (LL6; IW–1.9) (Schrader et al., 2016) formed under slightly more reducing conditions and contain only trace abundances of pentlandite.

The fO_2 recorded by both the Appley Bridge and Saint-Séverin LL6 chondrites are similar to one another. Although there are differences in the minor-element compositions of the troilite and pentlandite in these meteorites, we hypothesize that they are due to distinct thermal histories rather than the small difference in the fO_2 recorded by these materials. Therefore, compositional differences in troilite and pentlandite in these LL6 chondrites are most likely due to their distinct cooling histories.

Each LL chondrite studied here has fS_2 values above the IT buffer, IT+0.8 to IT+2.3 (Table 4). Of the samples studied here, Soko-Banja (LL4) was metamorphosed under the highest fS_2, while Siena (LL5) was the least sulfidized. These fS_2 values are consistent with the presence of troilite in each sample, and indicate that it is possible that 6C pyrrhotite could be present. Structural analysis of these sulfides is required to determine if 6C pyrrhotite is present.

CONCLUSIONS

This study shows that:

(1) The major and minor element compositions of pyrrhotite-group minerals (dominantly troilite) and pentlandite vary with the degree of thermal metamorphism. Therefore, chemical analyses of sulfides combined with petrographic observations can be used to determine the approximate petrographic type of the host LL chondrite.

(2) High degrees of shock on the LL parent body cause distinct textural, structural, and perhaps compositional changes (at S5; such as Chelyabinsk [LL5]) that can be used to identify highly shocked samples.

(3) The distinct pyrrhotite-pentlandite textures and minerals present in Appley Bridge [LL6]) may indicate that it cooled more slowly than the other metamorphosed LL chondrites studied here, potentially indicating it was more deeply buried on its parent asteroid.

(4) In order to learn more about the formation and alteration history of the LL chondrite parent body, this information can be applied to the study of other LL chondrites and to sulfides in samples of asteroid Itokawa returned by the Hayabusa mission (e.g., Schrader and Zega, 2018; 2019).

Acknowledgements.
For supplying the samples that were necessary for this work, the authors thank the Smithsonian Institution and the Arizona State University Center for Meteorite Studies. The authors thank Laurence Garvie for help with sample preparation. We thank Tim McCoy for helpful discussions and recommending Appley Bridge, Jemma Davidson for helpful discussions and manuscript editing, and Ken Domanik for helpful discussions about sulfides and for assistance with EPMA at UA. We are also grateful to Axel Wittmann for assistance with EPMA at ASU. We thank Alan Rubin, Dennis Harries, and associate editor Alexander Krot for constructive comments that significantly improved the quality of the manuscript. This work was funded by NASA grant NNX17AE53G (PI: DLS, CoI: TJZ).

Schrader D. L. and Zega T. J. (2019) Petrographic and compositional indicators of formation and alteration conditions from LL chondrite sulfides. *Geochim. Cosmochim. Acta* 264, 165–179.

REFERENCES

Anderson D. J., Lindsley D. H. and Davidson P. M. (1993) QUILF: A PASCAL program to assess equilibria among Fe–Mg–Ti oxides, pyroxenes, olivine, and quartz. *Comput. Geosci.* **19**, 1333–1350.

Arnold R. G. (1967) Range in composition and structure of 82 natural terrestrial pyrrhotites. *Can. Min.* **9**, 31–50.

Bayliss P. (1990) Revised unit-cell dimensions, space group, and chemical formula of some metallic minerals. *Can. Mineral.* **28**, 751–755.

Benedix G. K., Lauretta D. S. and McCoy T. J. (2005) Thermodynamic constraints on the formation conditions of winonaites and silicate-bearing IAB irons. *Geochim. Cosmochim. Acta* **69**, 5123–5131.

Bennett M. E. III and McSween H. Y. Jr (1996) Shock features in iron-nickel metal and troilite of L-group ordinary chondrites. *Meteorit. Planet. Sci.* **31**, 255–264.

Berger E. L., Zega T. J., Keller L. P., and Lauretta D. S. (2011) Evidence for aqueous activity on comet 81P/Wild 2 from sulfide mineral assemblages in Stardust samples and CI chondrites. *Geochim. Cosmochim. Acta* **75**, 3501–3513.

Berger E. L. and Keller L. P. (2015) A Hybrid Ultramicrotomy-FIB Technique for Preparing Serial Electron Transparent Thin Sections from Particulate Samples. *Microscopy Today* **23**, 18-23.

Bischoff A., Barrat J-A., Bauer K., Burkhardt C., Busemann H., Ebert S., Gonsior M., Hakenmüller J., Haoloda J., Harries D., Heinlein D., Hiesinger H., Hochleitner R., Hoffmann V., Kaliwoda M., Laubenstein M., Maden C., Meier M. M. M., Morlok A., Pack A., Ruf A., Schmitt-Kopplin P., Schönbächler M., Steele R. C. J., Spurný P., and Wimmer K. (2017) The Stubenberg meteorite—An LL6 chondrite fragmental breccia recovered soon after precise prediction of the strewn field. *Meteorit. Planet. Sci.* **52**, 1683–1703.

Brearley A. J. (2006) The Action of Water. In *Meteorites and the Early Solar System II* (eds. D. S. Lauretta and H. Y. McSween). University of Arizona Press, Tucson. pp. 584–624.

Bullock E. S., Gounelle M., Lauretta D. S., Grady M. M. and Russell S. S. (2005) Mineralogy and texture of Fe-Ni sulfides in CI1 chondrites: Clues to the extent of aqueous alteration on the CI1 parent body. *Geochim. Cosmochim. Acta* **69**, 2687–2700.

Busemann H., Alexander C. M. O'D. and Nittler L. R. (2007) Characterization of insoluble organic matter in primitive meteorites by microRaman spectroscopy. *Meteorit. Planet. Sci.* **42**, 1387–1416.

Chennaoui Aoudjehane H., El Goresy A., and Jambon A. (2007) The assemblage native copper, cobaltian kamacite and troilite in ordinary chondrites: Dissociation products not related to a shock event. *70th Annual Meeting of the Meteoritical Society* #5031.

Craig J. R., Naldrett A. J. and Kullerud G. (1968) The Fe-Ni-S system: 400°C isothermal diagram. *Carnegie I. Wash.* **66**, 440–441.

Etschmann B., Pring A., Putnis A., Grguric B. A. and Studer A. (2004) A kinetic study of the exsolution of pentlandite $(Ni,Fe)_9S_8$ from the monosulfide solid solution (Fe, Ni)S. *Am. Mineral.* **89**, 39–50.

Francis C. A., Fleet M. E., Misra K. and Craig J. R. (1976) Orientation of exsolved pentlandite in natural and synthetic nickeliferious pyrrhotite. *Am. Mineral.* **61**, 913–920.

Frazer J. Z., Keil K., and Reid A. M. (1969) Lattice parameters of kamacite by the Kossel technique. *Am. Mineral.* **54**, 554–559.

Gardner-Vandy K. G., Lauretta D. S., Greenwood R. C., McCoy T. J., Killgore M. and Franchi I. A. (2012) The Tafassassetprimitive achondrite: insights into initial stages of planetary differentiation. *Geochim. Cosmochim. Acta* **85**, 142–159.

Gardner-Vandy K. G., Lauretta D. S., and McCoy T. J. (2013) A petrologic, thermodynamic and experimental study of brachinites: Partial melt residues of an R chondrite-like precursor. *Geochim. Cosmochim. Acta* **122**, 36–57.

Ganguly J., Tirone M., Chakraborty S., and Domanik K. (2013) H-chondrite parent asteroid: A multistage cooling, fragmentation and re-accretion history constrained by thermometric studies, diffusion kinetic modeling and geochronological data. *Geochim. Cosmochim. Acta* **105**, 206–220.

Harries D. (2018) Sulfide mineralogy of heated CM/CI-like chondrites as indicator of asteroidal processes. *2018 Hayabusa Symposium* (abstract).

Harries D. and Langenhorst F. (2013) The nanoscale mineralogy of Fe,Ni sulfides in pristine and metamorphosed CM and CM/CI-like chondrites: Tapping a petrogenetic record. *Meteorit. Planet. Sci.* **48**, 879–903.

Harries D. and Langenhorst F. (2014) The mineralogy and space weathering of a regolith grain from 25143 Itokawa and the possibility of annealed solar wind damage. *Earth, Planets and Space* **55**, 163.

Harries D. and Zolensky M. E. (2016) Mineralogy of iron sulfides in CM1 and CI1 lithologies of the Kaidun breccia: Records of extreme to intense hydrothermal alteration. *Meteorit. Planet. Sci.* **51**, 1096–1109.

Harries D. and Langenhorst F. (2018) Carbide-metal assemblages in a sample returned from asteroid 25143 Itokawa: Evidence for methane-rich fluids during metamorphism. *Geochim. Cosmochim. Acta* **222**, 53–73.

Harries D., Pollock K., and Langenhorst F. (2011) Translation interface modulation in NC-pyrrhotites: Direct imaging by TEM and a model toward understanding partially disordered structural states. *American Mineralogist* **96**, 716–731.

Hirschmann M. M. (1991) Thermodynamics of multicomponent olivines and the solution properties of $(Ni,Mg,Fe)_2SiO_4$ and $(Ca,Mg,Fe)_2SiO_4$ olivines. *Am. Mineral.* **76**, 1232–1248.

Jamsja N. and Ruzicka A. (2010) Shock and thermal history of Northwest Africa 4859, an annealed impact-melt breccia of LL chondrite parentage containing unusual igneous features and pentlandite. *Meteorit. Planet. Sci.* **45**, 828–849.

Karup-Moeller S. and Makovicky E. (1995) The Phase System Fe-Ni-S at 725 °C, *Neues Jahr. Mineral. Monatsh.* **1**, 1–10.

Kaeter D., Ziemann M. A., Böttger U. Weber I., Hecht L., Voropaev S. A., Korochantsev A. V., and Kocherov A. V. (2018) The Chelyabinsk meteorite: New insights from a comprehensive electron microscopy and Raman spectroscopy study with evidence for graphite in olivine of ordinary chondrites *Meteorit. Planet. Sci.* **53**, 416–432.

Keil K., Zucolotto M. E., Krot A. N., Doyle P. M., Telus M., Krot T. V., Greenwood R. C., Franchi I. A., Wasson J. T., Welten K. C., Caffee M. W., Sears D. W. G., Riebe

M., Wieler R., Santos E., Scorzelli R. B., Gattacceca J., Lagroix F., Laubenstein M., Mendes J. C., Schmitt-Kopplin P., Harir M., and Moutinho A. L. R. (2015) The Vicência meteorite fall: A new unshocked (S1) weakly metamorphosed (3.2) LL chondrite. *Meteorit. Planet. Sci.* **50**, 1089–1111.

Kissin S. A. and Scott S. D. (1982) Phase relations involving pyrrhotite below 350°C. *Econ. Geol.* **77**, 1739–1754.

Kosyakov V. I., Sinyakova E. F. and Shestakov V. A. (2003) Dependence of sulfur fugacity on the composition of phase associations in the Fe–FeS–NiS–Ni system at 873 K. *Geochem. Int.* **7**, 660–669.

Kullerud G. (1963a) Thermal stability of pentlandite. *Can. Min.* **7**, 353–366.

Kullerud G. (1963b) The Fe-Ni-S system. *Annu. Rep. Geophys. Lab.* **1412**, 175–189. Washington, DC.

Kullerud G., Yund R. A., Moh G. (1969) Phase relations in the Fe-Ni-S, Cu-Fe-S, and Cu-Ni-S systems. *Econ. Geol. Monograph* **4**, 323–343.

Larimer J. W. (1968) Experimental studies on the system Fe–MgO–SiO_2–O_2 and their bearing on the petrology of chondritic meteorites. *Geochim. Cosmochim. Acta* **32**, 1187–1207.

Lauretta D. S., Lodders K. and Fegley Jr. B. (1998) Kamacite sulfurization in the solar nebula. *Meteorit. Planet. Sci.* **33**, 821–833.

Lauretta D. S., Buseck P. R., and Zega T. J. (2001) Opaque minerals in the matrix of the Bishunpur (LL3.1) chondrite: Constraints on the chondrule formation environment. *Geochim. Cosmochim. Acta* **65**, 1337–1353.

Lindsley D. H. (1983) Pyroxene thermometry. *Am. Mineral.* **68**, 477–493.

Makovicky E. (2006) Crystal structures of sulfides and other chalcogenides. In *Reviews in Mineralogy & Geochemistry Vol. 61* (ed. D. J. Vaughan). Geochemical Society, Mineralogical Society of America, pp. 7–125.

Matas J., Ricard Y., Lemelle L. and Guyot F. (2000) An improved thermodynamic model of metal–olivine–pyroxene stability domains. *Contrib. Mineral Petrol.* **140**, 73–83.

McSween H. Y. Jr. and Patchen A. D. (1989) Pyroxene thermobarometry in LL-group chondrites and implications for parent body metamorphism. *Meteoritics* **24**, 219–226.

McCoy T. J., Scott E. R. D., Jones R. H., Keil K. and Taylor G. J. (1991) Composition of chondrule silicates in LL3–5 chondrites and implications for their nebular history and parent body metamorphism. *Geochim. Cosmochim. Acta* **55**, 601–619.

McCoy T. J., Mittlefehldt D. W. and Wilson L. (2006) Asteroid differentiation. In *Meteorites and the Early Solar System II* (eds. D. S. Lauretta and H. Y. McSween). University of Arizona Press, Tucson. pp. 733–745.

Mengason M. J., Piccoli P. M., and Candela P. (2010) An evaluation of the effect of copper on the estimation of sulfur fugacity (fS_2) from pyrrhotite composition. *Econ. Geol.* **105**, 1163–1169.

Misra K. C. and Fleet M. E. (1973) The chemical compositions of synthetic and natural pentlandite assemblages. *Econ. Geol.* **68**, 518–539.

Morimoto N., Gyobu A., Mukaiyama H., and Izawa E. (1975) Crystallography and stability of pyrrhotites. *Econ. Geo.* **70**, 824-833.

Nakamura T., Noguchi T., Tanaka M., Zolensky M. E., Kimura M., Tsuchiyama A., Nakato A., Ogami T., Ishida H., Uesugi M., Yada T., Shirai K., Fujimura A., Okazaki R., Sandford S. A., Ishibashi Y., Abe M., Okada T., Ueno M., Mukai T., Yoshikawa

M. and Kawaguchi J. (2011) Itokawa Dust Particles: A Direct Link Between S-Type Asteroids and Ordinary Chondrites. *Science* **333**, 1113–1116.

Nakamuta Y., Urata K., Shibata Y., and Kuwahara Y. (2017) Effect of $NaCrSi_2O_6$ component on Lindsley's pyroxene thermometer: An evaluation based on strongly metamorphosed LL chondrites. *Meteorit. Planet. Sci.* **52**, 511–521.

Naldrett A. J., Craig J. R., and Kullerud G. (1967) The central portion of the Fe-Ni-S system and its bearing on pentlandite exsolution in iron-nickel sulfide ores. *Econ. Geol*. **62**, 826–847.

Naldrett A. J. (1989) *Magmatic Sulphide Deposits*. Oxford University Press, Oxford.

Noguchi T., Nakamura T., Kimura M., Zolensky M. E., Tanaka M., Hashimoto T., Konno M., Nakato A., Ogami T., Fujimura A., Abe M., Yada T., Mukai T., Ueno M., Okada T., Shirai K., Ishibashi Y., and Okazaki R. (2011) Incipient space weathering observed on the surface of Itokawa dust particles. *Science* **333**, 1121–1125.

Noguchi T., Bridges J. C., Hicks L. J., Gurman S. J., Kimura M., Hashimoto T., Konno M., Bradley J. P., Okazaki R., Uesugi M., Yada T., Karouji Y., Abe M., Okada T., Mitsunari T., Nakamura T., and Kagi H. (2014) Mineralogy of four Itokawa particles collected from the first touchdown site. *Earth, Planets and Space* **66**, 124.

Raghavan V. (2004) Fe–Ni–S (iron–nickel–sulfur). *J. Phase Equilib.* **25**, 373–381.

Rubin A. E. (1990) Kamacite and olivine in ordinary chondrites: Intergroup and intragroup relationships. *Geochim. Cosmochim. Acta* **54**, 1217–1232.

Rubin A. E. (2004) Postshock annealing and postannealing shock in equilibrated ordinary chondrites: Implications for the thermal and shock histories of chondritic asteroids. *Geochim. Cosmochim. Acta* **68**, 673–689.

Ruzicka A., Grossman J., Bouvier A., Herd C. D. K., and Agee C. B. (2015) The Meteoritical Bulletin, No. 102. *Meteorit. Planet. Sci.* **50**, 1662.

Sack R. O. and Ghiorso M. S. (1989) Importance of considerations of mixing properties in establishing an internally consistent database: Thermochemistry of minerals in the system Mg_2SiO_4–Fe_2SiO_4–SiO_2. *Contrib. Mineral. Petrol.* **102**, 41–68.

Singerling S. A. and Brearley A. J. (2018) Primary iron sulfides in CM and CR carbonaceous chondrites: Insights into nebular processes. *Meteorit. Planet. Sci.* **53**, 2078–2106.

Schmitt R. T., Deutsch A., and Stöffler D. (1993) Shock effects in experimentally shocked samples of the H6 chondrite Kernouve (abstract). *Meteoritics* 28, 431–432.

Schrader D. L. and Zega T. J. (2018) Preliminary results from sulfide Hayabusa particle RB-CV-0234. *Hayabusa 2018, 6th Symposium on Solar System Materials.*

Schrader D. L. and Zega T. J. (2019) Comparison of the sulfide-bearing Hayabusa particles RB-CV-0234 and RB-QD04-0039 to LL chondrite sulfides. Lunar Planet. Sci. L. Lunar Planet. Inst., Houston. #2009 (abstr.).

Schrader D. L., Connolly H. C. Jr., Lauretta D. S., Nagashima K., Huss G. R., Davidson J. and Domanik K. J. (2013) The formation and alteration of the Renazzo-like carbonaceous chondrites II: Linking O-isotope composition and oxidation state of chondrule olivine. *Geochim. Cosmochim. Acta.* **101**, 302–327.

Schrader D. L., Davidson J., Greenwood R. C., Franchi I. A., and Gibson J. M. (2014) A water-ice rich minor body from the early Solar System: The CR chondrite parent asteroid. Earth Planet. Sci. Lett. 407, 48–60.

Schrader D. L., Connolly H. C. Jr., Lauretta D. S., Zega T. J., Davidson J. and Domanik K. J. (2015) The formation and alteration of the Renazzo-like carbonaceous chondrites III: Toward understanding the genesis of ferromagnesian chondrules. *Meteorit. Planet. Sci.* **50**, 15–50.

Schrader D. L., Davidson J., and McCoy T. J. (2016) Widespread evidence for high-temperature formation of pentlandite in chondrites. *Geochim. Cosmochim. Acta* **189**, 359–376.

Schrader D. L., McCoy T. J., and Gardner-Vandy K. (2017) Relict chondrules in primitive achondrites: Remnants from their precursor parent bodies. *Geochim. Cosmochim. Acta.* **205**, 295–312.

Schrader D. L., Fu R. R., Desch S. J., and Davidson J. (2018) The background temperature of the protoplanetary disk within the first four million years of the Solar System. *Earth Planet. Sci. Lett.* **504**, 30–37.

Shewman R. W. and Clark L. A. (1970) Pentlandite phase relations in the Fe-Ni-S system and notes on the monosulfide solid solution. *C and. J. Earth Sci.* **7**, 67–85.

Slater-Reynolds V. and McSween H. Y. (2005) Peak metamorphic temperatures in type 6 ordinary chondrites: An evaluation of pyroxene and plagioclase geothermometry. *Meteorit. Planet. Sci.* **40**, 745–754.

Stöffler D., Keil K., and Scott E. R. D. (1991) Shock metamorphism of ordinary chondrites. *Geochim. Cosmochim. Acta* **55**, 3845–3867.

Sugaki A. and Kitakaze A. (1998) High form pentlandite and its thermal stability. *Am. Mineral.* **83**, 133–140.

Tachibana S. and Huss G. R. (2005) Sulfur isotope composition of putative primary troilite in chondrules from Bishunpur and Semarkona. *Geochim. Cosmochim. Acta* **69**, 3075–3097.

Tachibana S., Nagahara H., and Mizuno K. (2006) Constraints on cooling rates of chondrules from metal-troilite assemblages (Abstract #2263). In: 37th Lunar and Planetary Science Conference, CD-ROM.

Toulmin P. III and Barton P. B. Jr. (1964) A thermodynamic study of pyrite and pyrrhotite. *Geochim. Cosmochim. Acta* **28**, 641–671.

Tsuchiyama A., Uesugi M., Matsushima T., Michikami T., Kadono T., Nakamura T., Uesugi K., Nakano T., Sandford S. A., Noguchi R., Matsumoto T., Matsuno J., Nagano T., Imai Y., Takeuchi A., Suzuki Y., Ogami T., Katagiri J., Ebihara M., Ireland T. R., Kitajima F., Nagao K., Naraoka H., Noguchi T., Okazaki R., Yurimoto H., Zolensky M. E., Mukai T., Abe M., Yada T., Fujimura A., Yoshikawa M., and Kawaguchi J. (2011) Three-Dimensional Structure of Hayabusa Samples: Origin and Evolution of Itokawa Regolith. *Science* **333**, 1125–1128.

Tsuchiyama A., Uesugi M., Uesugi K., Nakano T., Noguchi R., Matsumoto T., Matsuno J., Nagano T., Imai Y., Shimada A., Takeuchi A., Suzuki Y., Nakamura T., Noguchi T., Abe M., Yada T., and Fujimura A. (2014) Three-dimensional microstructure of samples recovered from asteroid 25143 Itokawa: Comparison with LL5 and LL6 chondrite particles. *Meteorit. Planet. Sci.* **49**, 172–187.

Wang H., Pring A., Wu F., Chen G., Jiang J., Xia F., Zhang J., Ngothai Y., and O'Neill B. (2006) Effect of cation vacancy and crystal superstructure on thermodynamics of iron monosulfides. *Journal of Sulfur Chemistry* **27**, 1–12.

Waldner P. and Pelton A. D. (2004) Critical thermodynamic assessment and modeling of the Fe-Ni-S system. *Metall. Mater. Trans. B* **35B**, 897–907.

Waldner P. and Sitte W. (2008) Thermodynamic modeling of Fe-Ni pentlandite. *J. Phys. Chem. Solids* **69**, 923–927.

Weisberg M. K., McCoy T. J. and Krot A. N. (2006) Systematics and evaluation of meteorite classification. In Meteorites and the Early Solar System II (eds. D. S. Lauretta and H. Y. McSween). University of Arizona Press, Tucson, pp. 19–52.

Zolensky M. E., Nakamura T., Mikouchi T., Hagiya K., Ohsumi K., Tanaka M., Noguchi T., Kimura M., Tsuchiyama A., Nakato A., Ogami T., Ishida H., Uesugi M., Yada T., Shirai K., Fujimura A., Okazaki R., Ishibashi Y., Abe M., Okada T., Ueno M., Mukai T., Yoshikawa M., and Kawaguchi J. (2012) The shock state of Itokawa samples. Lunar Planet. Sci. XLIII. Lunar Planet. Inst., Houston. #1477 (abstr.).

TABLES

Table 1. LL chondrites studied

Meteorite Name	Type	Shock Stage	Reference	Fall	Year
Semarkona USNM1805-17	LL3.00	S2	1,2	Y	1940
Vicência ASU1996	LL3.2	S1	2,3	Y	2013
Hamlet ASU1194_C_2	LL4	S3	1	Y	1959
Soko-Banja USNM3078-1	LL4	S3	2	Y	1877
Chelyabinsk ASU1801_22_C1	LL5	S5	2	Y	2013
Siena USNM3070-3	LL5	S3/4	2	Y	1794
Appley Bridge USNM614-3	LL6	S3	2	Y	1914
Saint-Séverin USNM2608-3	LL6	S2	2,4	Y	1966

(1) Stöffler et al. (1991); (2) this study; (3) Keil et al. (2015); (4) Rubin (2004); Y = yes

Po = pyrrhotite; Pn = pentlandite

Table 2. Mean sulfide compositions (wt.%)

Meteorite Name	Type	Mineral		Fe	S	Ni	Co	Cr	P	Cu	Total	# Analyses
Troilite (Ni-poor pyrrhotite)												
Semarkona USNM1805-17	LL3.00	Po	avg±stdev	63.1±0.4	36.8±0.2	0.12±0.20	bdl	0.04±0.03	bdl	bdl	100.0±0.4	29
			min–max	62.4–63.8	36.4–37.2	bdl–0.90	bdl	bdl–0.08	bdl	bdl	99.2–101.0	
Vicência ASU1996	LL3.2	Po	avg±stdev	63.2±0.3	36.6±0.2	0.03±0.09	bdl	0.03±0.06	bdl	0.10±0.11	100.1±0.4	22
			min–max	62.1–63.9	36.1–37.1	bdl–0.37	bdl	bdl–0.25	bdl	bdl–0.32	99.2–100.8	
Hamlet ASU1194_C_2	LL4	Po	avg±stdev	63.4±0.2	36.8±0.2	0.05±0.09	bdl	0.01±0.21	bdl	bdl	100.4±0.3	18
			min–max	63.0–63.9	36.6–37.2	bdl–0.27	bdl	bdl–0.05	bdl	bdl	99.9–100.9	
Soko-Banja USNM3078-1	LL4	Po	avg±stdev	63.4±0.5	37.2±0.2	0.00±0.01	bdl	0.01±0.03	bdl	bdl	100.6±0.7	38
			min–max	62.2–64.3	36.7–37.6	bdl–0.05	bdl	bdl–0.09	bdl	bdl	99.0–101.8	
Chelyabinsk ASU1801_22_C1	LL5	Po	avg±stdev	63.1±0.5	36.8±0.2	0.16±0.13	bdl	bdl	bdl	0.05±0.19	100.1±0.6	22
			min–max	62.2–64.3	36.5–37.1	bdl–0.58	bdl	bdl	bdl	bdl–0.88	99.2–101.6	
Siena USNM3070-3	LL5	Po	avg±stdev	63.2±0.6	36.5±0.3	0.05±0.08	0.03±0.06	bdl	0.01±0.03	bdl	99.9±0.6	5
			min–max	62.1–63.8	35.8–37.0	bdl–0.16	bdl–0.14	bdl	bdl–0.07	bdl	98.5–100.5	
Appley Bridge USNM614-3	LL6	Po	avg±stdev	63.4±0.3	36.6±0.1	0.07±0.11	bdl	bdl	bdl	0.07±0.19	100.2±0.2	12
			min–max	62.8–63.9	36.4–36.7	bdl–0.29	bdl	bdl	bdl	bdl–0.66	99.8–100.6	
Saint-Séverin USNM2608-3	LL6	Po	avg±stdev	63.1±0.8	36.8±0.4	0.03±0.05	bdl	bdl	bdl	bdl	99.9±1.1	11
			min–max	61.8–64.0	36.1–37.8	bdl–0.15	bdl	bdl	bdl	bdl	98.3–101.8	
Ni-rich pyrrhotite (16>Ni>1 wt.%)												
Semarkona USNM1805-17	LL3.00	Ni-rich po	avg±stdev	52.8±4.1	34.2±1.1	11.8±5.1	0.30±0.17	0.07±0.07	0.01±0.02	0.08±0.08	99.4±1.0	7
			min–max	49.3–61.4	32.8–36.3	1.11–15.4	bdl–0.52	bdl–0.21	bdl–0.05	bdl–0.18	98.2–101.2	
Vicência ASU1996	LL3.2	Ni-rich po	avg±stdev	55.9±7.1	34.9±1.7	8.5±7.6	0.14±0.07	0.16±0.09	bdl	0.22±0.06	100.0±0.8	2
			min–max	50.8–60.9	33.7–36.1	3.2–13.9	0.09–0.19	0.09–0.22	bdl	0.18–0.26	99.5–100.6	
Hamlet ASU1194_C_2	LL4	Ni-rich po	avg±stdev	55.2±7.6	35.4±1.3	9.0±9.5	0.39±0.08	bdl	bdl	bdl	100.0±0.6	2
			min–max	49.8–60.6	34.5–36.3	2.3–15.7	0.33–0.45	bdl	bdl	bdl	99.5–100.4	
Soko-Banja USNM3078-1	LL4	Ni-rich po	avg±stdev	60.3	36.2	1.8	bdl	0.05	bdl	bdl	98.7	1
			min–max	-	-	-	-	-	-	-	-	
Appley Bridge USNM614-3	LL6	Ni-rich po	avg±stdev	56.8±4.4	35.2±0.8	6.6±5.2	0.40±0.27	bdl	bdl	1.26±1.05	100.2±1.0	15
			min–max	49.6–62.0	34.0–36.2	1.17–15.8	bdl–0.88	bdl	bdl	bdl–4.11	98.3–101.7	
Saint-Séverin USNM2608-3	LL6	Ni-rich po	avg±stdev	56.1±1.8	35.0±0.3	8.09±3.56	0.11±0.16	bdl	bdl	0.18±0.25	99.5±1.4	2
			min–max	54.9–57.4	34.8–35.2	5.57–10.6	bdl–0.23	bdl	bdl	bdl–0.36	98.5–100.5	
Pentlandite												
Semarkona USNM1805-17	LL3.00	Pn	avg±stdev	47.6±0.8	33.9±0.4	17.6±0.6	0.39±0.15	0.03±0.04	0.01±0.03	0.11±0.09	99.6±0.8	24
			min–max	46.1–50.1	33.2–34.7	16.0–18.5	0.12–0.63	bdl–0.19	bdl–0.13	bdl–0.29	98.0–101.0	
Vicência ASU1996	LL3.2	Pn	avg±stdev	46.0±1.5	33.5±0.5	18.8±1.4	0.61±0.20	0.02±0.05	bdl	0.14±0.14	99.2±0.6	7
			min–max	44.7–48.9	32.6–34.0	16.3–20.5	0.20–0.78	bdl–0.12	bdl	bdl–0.33	98.2–99.8	
Hamlet ASU1194_C_2	LL4	Pn	avg±stdev	46.5±1.1	34.0±0.4	18.9±1.3	0.77±0.55	bdl	bdl	0.05±0.07	100.1±0.7	8
			min–max	44.8–48.7	33.5–34.6	17.4–21.3	0.37–2.02	bdl	bdl	bdl–0.13	99.1–101.2	
Soko-Banja USNM3078-1	LL4	Pn	avg±stdev	46.7±1.3	33.9±0.6	18.0±1.1	0.31±0.28	0.03±0.06	bdl	0.31±0.18	99.3±0.8	11
			min–max	45.3–49.3	33.0–34.9	16.1–19.7	bdl–0.82	bdl–0.15	bdl	0.14–0.68	98.1–100.9	
Chelyabinsk ASU1801_22_C1	LL5	Pn	avg±stdev	45.2±0.4	33.4±0.2	18.5±1.0	0.05±0.08	bdl	bdl	1.73±1.13	99.0±0.4	6
			min–max	44.8–45.6	33.1–33.6	17.2–19.6	bdl–0.16	bdl	bdl	0.32–2.82	98.4–99.4	
Siena USNM3070-3	LL5	Pn	avg±stdev	43.3±2.0	33.7±0.4	21.4±1.6	0.63±0.40	0.03±0.11	bdl±0.01	0.10±0.20	99.2±0.9	15
			min–max	39.7–46.5	33.0–34.2	19.0–23.7	bdl–1.14	bdl–0.41	bdl–0.04	bdl–0.76	98.2–101.6	
Appley Bridge USNM614-3	LL6	Pn	avg±stdev	47.0±0.5	33.4±0.2	17.8±0.5	0.57±0.12	bdl	bdl	0.92±0.47	99.6±0.4	20
			min–max	45.8–48.1	33.1–34.2	17.0–18.8	0.42–0.86	bdl	bdl	0.26–1.77	98.9–100.5	
Saint-Séverin USNM2608-3	LL6	Pn	avg±stdev	43.7±1.3	33.7±0.3	20.4±1.5	0.85±0.63	bdl	bdl±0.01	0.13±0.29	98.8±0.7	25
			min–max	40.9–46.2	33.1–34.2	17.2–23.1	bdl–2.41	bdl	bdl–0.03	bdl–1.19	98.0–101.1	

Po = pyrrhotite, Pn = pentlandite; avg = average; stdev = standard deviation; bdl = below detection limit. Detection limits listed in EA-1.

Table 3. Average olivine and pyroxene compositions from Appley Bridge (wt.%)

Element	Olivine	LCP	HCP
# Analyses	n=5	n=2	n=4
Source	this study	this study	McSween and Patchen (1989)
SiO_2	36.65	54.18	53.95
TiO_2	bdl	0.19	0.45
Al_2O_3	bdl	0.16	0.49
Cr_2O_3	0.04	0.13	0.77
P_2O_5	0.06	bdl	bdl
MgO	34.81	26.85	15.94
CaO	bdl	0.90	21.22
MnO	0.44	0.47	0.21
FeO	27.66	16.73	6.41
NiO	0.23	bdl	bdl
Na_2O	bdl	bdl	0.54
Total	99.82	99.68	99.98
Fa or Fs	30.8	25.4	10.3
Fo or En	69.2	72.8	45.8
Wo	-	1.7	43.8
Two-pyroxene temperature (±2σ)	-	913±36°C	

LCP = low calcium pyroxene; HCP = high calcium pyroxene.

n = number of analyses; bdl = below detection limit.

Standards and detection limits for this study (in wt.%): albite for Na (0.03), diopside for Si (0.02), Mg (0.04), and Ca (0.01), anorthite for Al (0.02), orthoclase for K (0.02), rhodonite for Mn (0.05), rutile for Ti (0.02), fayalite for Fe (0.07), chromite for Cr (0.02), and nickel metal for Ni (0.07).

K was bdl.

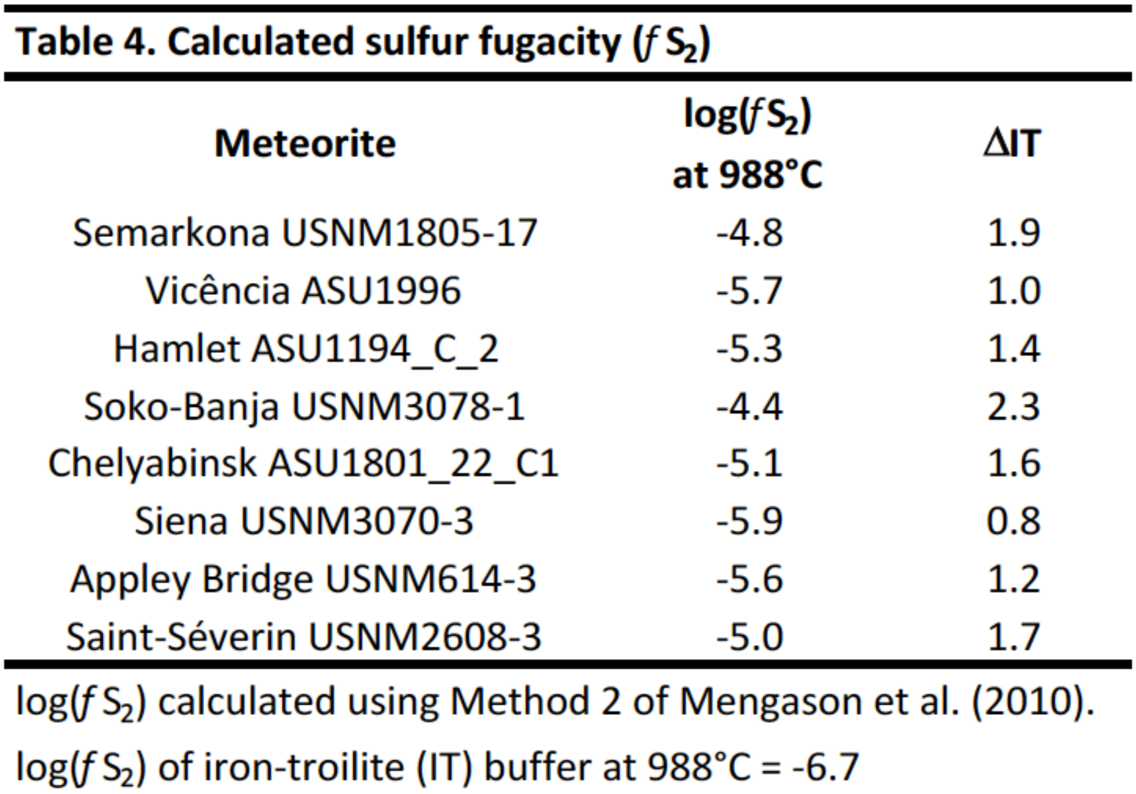

Table 4. Calculated sulfur fugacity (fS_2)

Meteorite	$\log(fS_2)$ at 988°C	ΔIT
Semarkona USNM1805-17	-4.8	1.9
Vicência ASU1996	-5.7	1.0
Hamlet ASU1194_C_2	-5.3	1.4
Soko-Banja USNM3078-1	-4.4	2.3
Chelyabinsk ASU1801_22_C1	-5.1	1.6
Siena USNM3070-3	-5.9	0.8
Appley Bridge USNM614-3	-5.6	1.2
Saint-Séverin USNM2608-3	-5.0	1.7

$\log(fS_2)$ calculated using Method 2 of Mengason et al. (2010).

$\log(fS_2)$ of iron-troilite (IT) buffer at 988°C = -6.7

FIGURES

Figure 1.

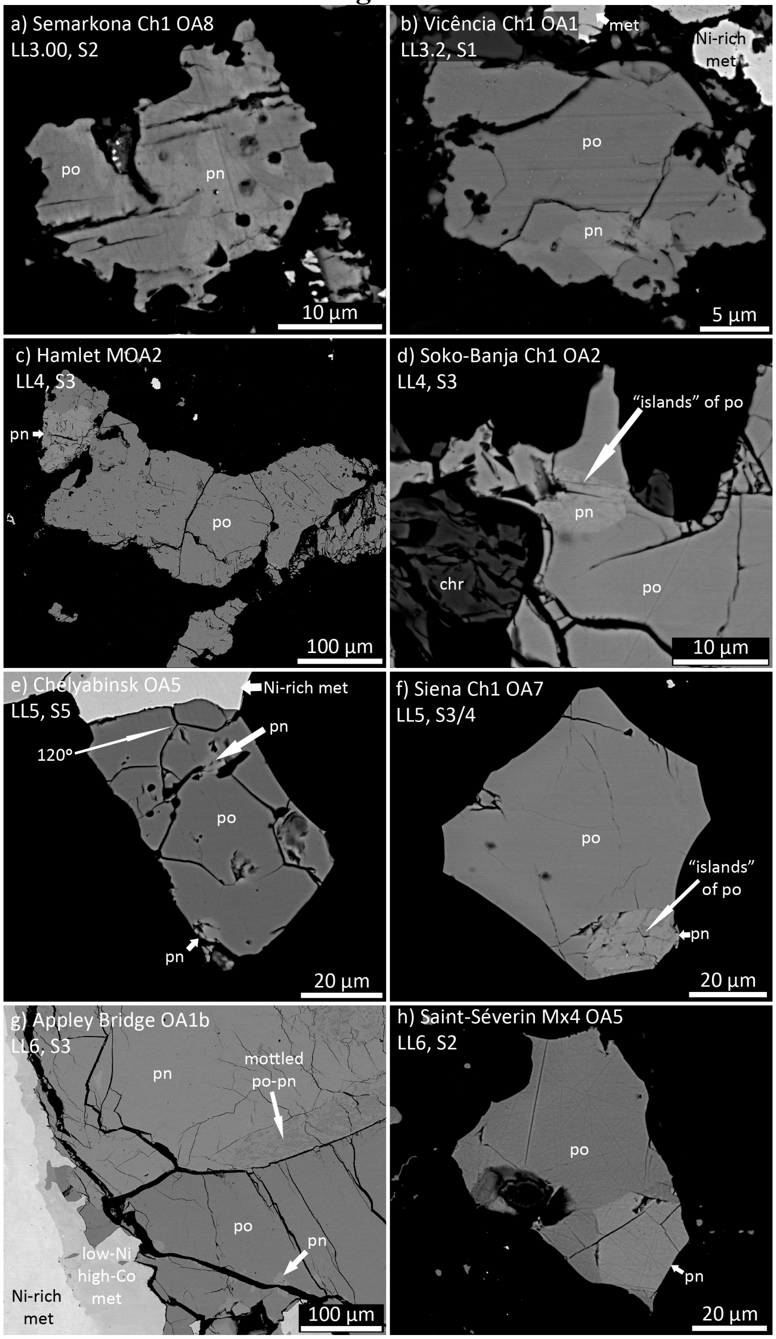

Figure 1. BSE images of sulfides containing pyrrhotite (po) – pentlandite (pn) intergrowths in (a) Semarkona (LL3.00, S2), (b) Vicência (LL3.2, S1), (c) Hamlet (LL4, S3), (d) Soko-Banja (LL4, S3), (e) Chelyabinsk (LL5, S5), (f) Siena (LL5, S3/4), (g) Appley Bridge (LL6, S3), and (h) Saint-Séverin (LL6, S2). The pyrrhotite (po) in Chelyabinsk (e) displays multiple 120° triple junctions. Where: Ch = chondrule; OA = opaque assemblage; MOA = matrix opaque assemblage; Mx = matrix; met = Fe,Ni metal; chr = chromite.

Figure 2.

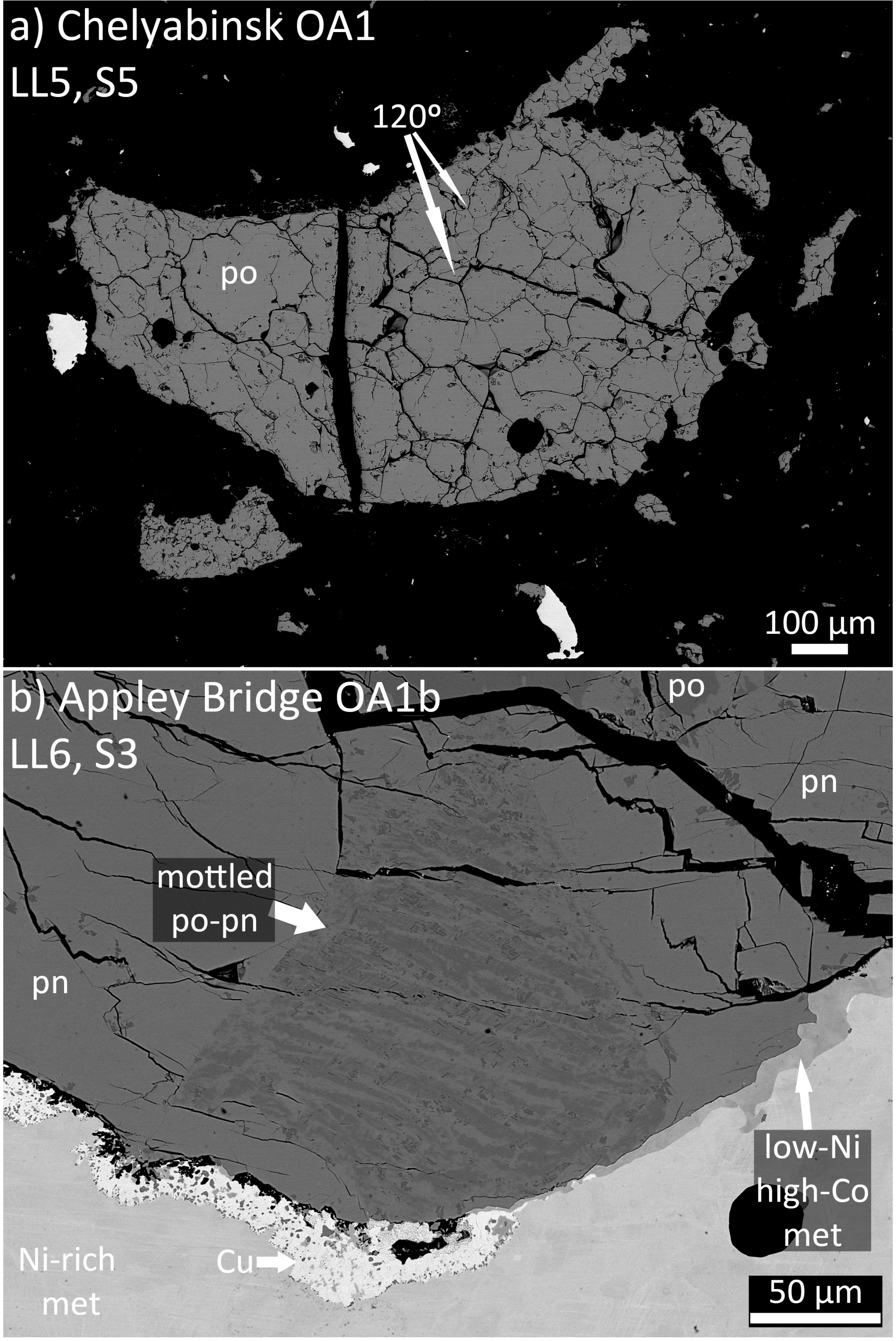

Figure 2. BSE images of uncommon sulfide textures and associated minerals in (a) Chelyabinsk (LL5, S5) and (b) Appley Bridge (LL6, S3). The grain of pyrrhotite (po) in Chelyabinsk (a) contains numerous 120° triple junctions. (b) Appley Bridge contains regions of 'mottled' pyrrhotite-pentlandite (pn) intergrowths, which border larger regions of po and pn, as well as metallic Cu, Ni-rich metal (met), and a low-Ni high-Co metal. Where: OA = opaque assemblage.

Figure 3.

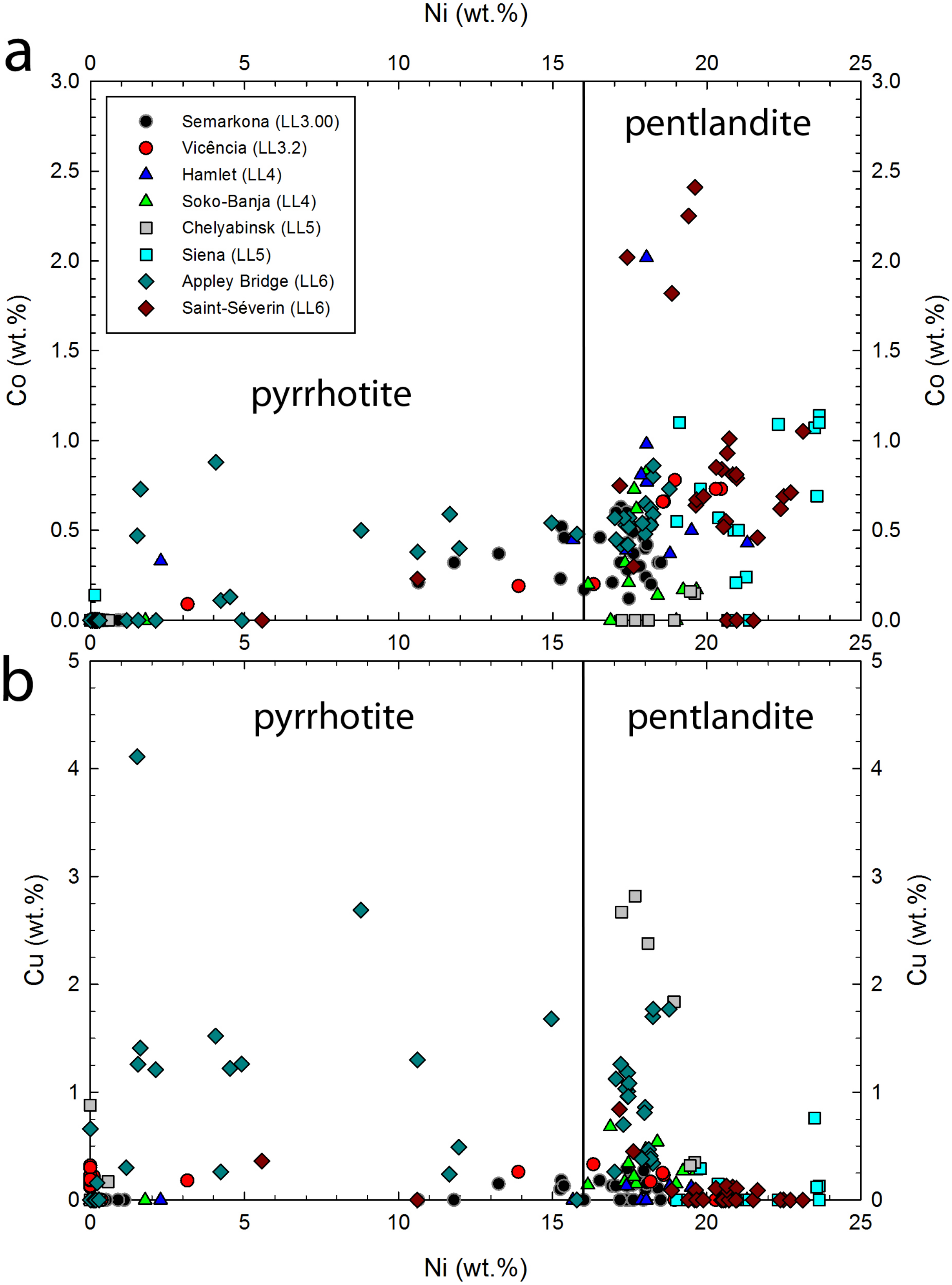

Figure 3. (a) Ni vs. Co (wt.%) and (b) Ni vs. Cu (wt.%) compositions of sulfides. Analyses along the x- and y-axes are below the element's detection limit (Table EA-1). The vertical line is the compositional boundary between pyrrhotite and pentlandite.

Figure 4.

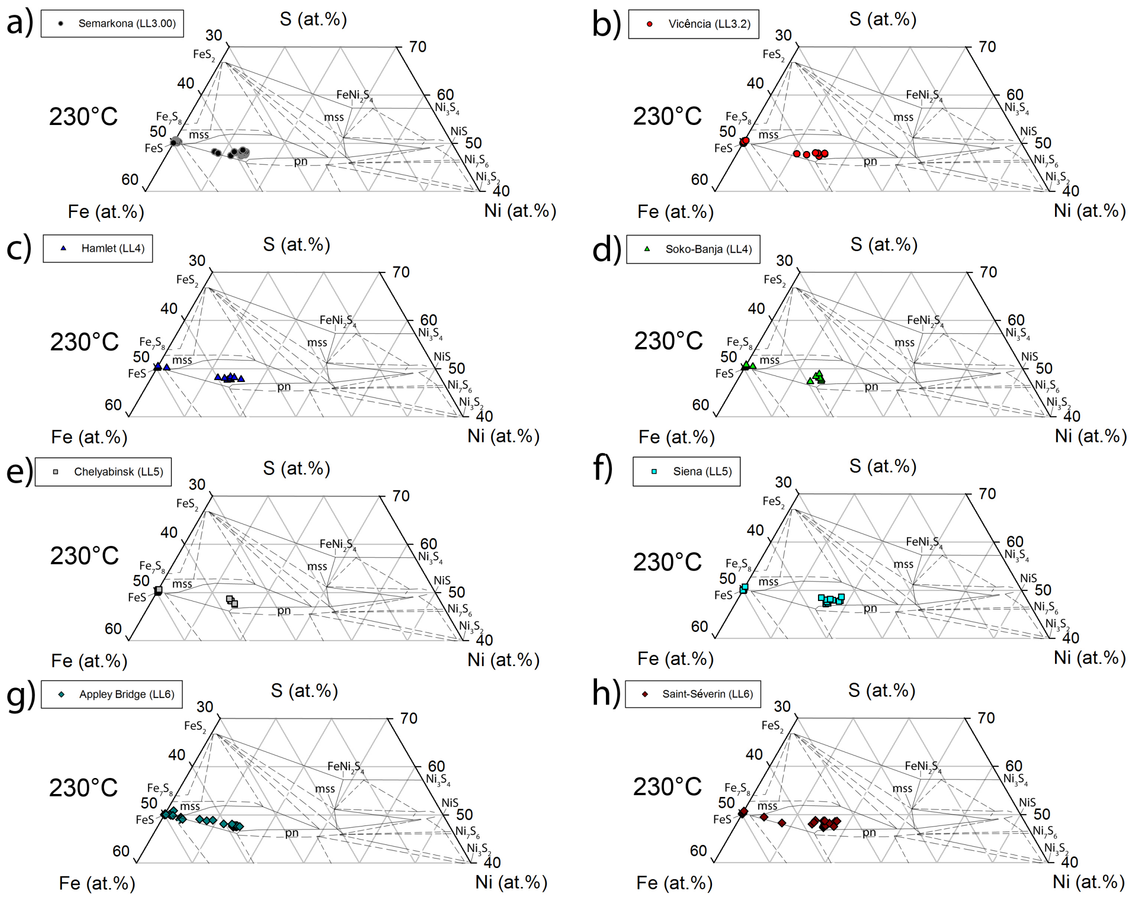

Figure 4. Fe-Ni-S ternary phase diagrams that most closely match the sulfides data from each LL chondrite studied here: (a) Semarkona (LL3.00, S2); (b) Vicência (LL3.2, S1), (c) Hamlet (LL4, S3); (d) Soko-Banja (LL4, S3); (e) Chelyabinsk (LL5, S5); (f) Siena (LL5, S3/4); (g) Appley Bridge (LL6, S3); and (h) Saint-Séverin (LL6, S2). All LL chondrite sulfides studied here are consistent with equilibrating at ≤230°C; since pentlandite in each sample is near the pentlandite stability field and troilite is along the tie line between troilite and the pentlandite field. Since pentlandite in each sample is near but more Ni-poor than the stability field, the equilibration temperature is ≤230°C. Where pn = pentlandite and mss = monosulfide solid solution. Phase diagrams adapted from Raghavan (2004); original data for 230 °C diagram from Misra and Fleet (1973).